Asian Journal of Pharmaceutical Sciences 14 (2019) 569–580

Available online at www.sciencedirect.com

ScienceDirect

journal homepage: www.elsevier.com/locate/AJPS

Original Research Paper

Triphenylphosphonium-modified mitochondria-targeted paclitaxel nanocrystals for overcoming multidrug resistance

*Xue Han, Ruijuan Su, Xiuqing Huang, Yingli Wang, Xiao Kuang, Shuang Zhou, Hongzhuo Liu**

Shenyang Pharmaceutical University, Shenyang 110016, China

ARTICLE INFO

Article history:
Received 25 April 2018
Revised 23 May 2018
Accepted 6 June 2018
Available online 18 September 2018

Keywords:
Paclitaxel
Nanocrystals
Brij 98
Triphenylphosphonium
Multidrug resistance
Mitochondria

ABSTRACT

Mitochondria are currently known as novel targets for treating cancer, especially for tumors displaying multidrug resistance (MDR). This present study aimed to develop a mitochondria-targeted delivery system by using triphenylphosphonium cation (TPP^+)-conjugated Brij 98 as the functional stabilizer to modify paclitaxel (PTX) nanocrystals (NCs) against drug-resistant cancer cells. Evaluations were performed on 2D monolayer and 3D multicellular spheroids (MCs) of MCF-7 cells and MCF-7/ADR cells. In comparison with free PTX and the non-targeted PTX NCs, the targeted PTX NCs showed the strongest cytotoxicity against both 2D MCF-7 and MCF-7/ADR cells, which was correlated with decreased mitochondrial membrane potential. The targeted PTX NCs exhibited deeper penetration on MCF-7 MCs and more significant growth inhibition on both MCF-7 and MCF-7/ADR MCs. The proposed strategy indicated that the TPP^+-modified NCs represent a potentially viable approach for targeted chemotherapeutic molecules to mitochondria. This strategy might provide promising therapeutic outcomes to overcome MDR.

1. Introduction

Multidrug resistance (MDR) remains a huge obstacle to successful chemotherapy in clinical cancer treatment. Although combination anti-tumor therapy restricts the chance of MDR to some extent, unsatisfactory therapeutic outcomes and side effects due to the different pharmacokinetic profiles of individual therapeutic molecules are the leading cause of combined chemotherapy failure [1–3].

Drug efflux transporters are some of the most-characterized mechanisms of MDR. Among them, P-glycoprotein (P-gp), belonging to the efflux ATP-binding cassette (ABC) transporters, was recognized as part of a major route for pumping out intracellular chemotherapeutic agents

* Corresponding author at: Shenyang Pharmaceutical University, No. 103, Wenhua Road, Shenyang 110016, China. Tel.: +86 24 43520586.
E-mail address: liuhongzhuo@syphu.edu.cn (H. Liu).
Peer review under responsibility of Shenyang Pharmaceutical University.

https://doi.org/10.1016/j.ajps.2018.06.006

[3–5]. Accordingly, an increasing number of strategies have been proposed to overcome MDR via evading or inhibiting P-gp to improve the therapeutic index of chemotherapy. For example, combining anticancer drugs with a P-gp inhibitor, such as verapamil [6, 7], tetrandrin [4, 8], or D-α-tocopherol polyethylene glycol succinate (TPGS) [9, 10] in one drug delivery platform has been used to overcome P-gp-mediated efflux in many preclinical and clinical studies. In our previous work, we demonstrated that TPGS improved the accumulation of paclitaxel (PTX) in drug-resistant tumors compared to Taxol® [11]. Similarly, some other nonionic surfactants, such as Brij, were shown to increase PTX accumulation in the MDR cell line (H460/taxR cells) and restore therapeutic sensitivity to those cells [12].

Recently, several researchers revealed that mitochondria-targeted agents/delivery systems could hinder the pumping activity of efflux transporters by depleting intracellular ATP levels and decreasing the mitochondrial membrane potential (MMP, $\Delta\Psi m$) in cancer cells [13–16]. Triphenylphosphonium cation (TPP^+), mitochondrial homing moiety with high lipophilicity, served as the frequently-used targeted moiety. For example, by attaching TPP^+ as the mitochondrial homing moiety to α-tocopherol succinate, mito-vitamin E was shown to overcome drug resistance in lung carcinoma [17]. Furthermore, TPP^+-modified PTX loaded liposomes exhibited enhanced cytotoxic effects in PTX-resistant human ovarian carcinoma cells and lung carcinoma [18, 19]. And doxorubicin (DOX) loaded TPP^+-functionalized polydopamine nanoparticles was also developed and demonstrated improved potency to overcome MDR when compared to that of the regular formulations [20]. In another study, DOX was conjugated to TPP^+ that was selectively taken up by mitochondria and significantly decreased IC_{50} of DOX in MDA-MB-435/DOX cells [21]. Here, we hypothesized that modification Brij with TPP^+ to synthesize dual functional copolymer which was equipped with P-gp inhibition effect and mitochondrial targeting delivery would provide synergistic potential for overcoming MDR in PTX. To improve the drug loading capacity, PTX nanocrystals (NCs) stabilized with TPP^+-modified Brij 98 (B-TPP) were developed and then their therapeutic effects were evaluated. The results of this study demonstrated that the mitochondria-targeted PTX NCs exhibited higher efficacy in MCF-7/ADR, a PTX-resistant cell line, and deeper tumor penetration in a model of MCF-7 multicellular spheroids (MCs) and more significant growth inhibition in both MCF-7 MCs and MCF-7/ADR MCs.

2. Materials and methods

2.1. Materials

Brij 98 and coumarin-6 were purchased from Sigma Aldrich (St. Louis, MO, USA). Paclitaxel (PTX) was purchased from Nanjing Jingzhu Biotechnology Co. Ltd. (Nanjing, China). 5-Carboxypentyl triphenylphosphonium (TPP), 1-hydroxybenzotriazole (HOBT), 1-ethyl-(3-dimethylaminopropyl)carbodiimide hydrochloride (EDCI), and 4-dimethylaminopyridine (DMAP) were all obtained from Beijing Ouhe Technology Co. Ltd. (Beijing, China). Tetramethylrhodamine ethyl ester (TMRE) and Mitotracke Red were purchased from Yeasenpharma Co. Ltd. (Shanghai, China). Carbonyl cyanide-p-trifluoromethoxyphenylhydrazone (FCCP) was purchased from Santa Cruz Biotechnology (Santa Cruz, CA, USA). 3-(4,5-dimethylthiazol-2-yl)-2,5-diphenyltetrazolium bromide (MTT) was purchased from Melonepharma Co. Ltd. (Dalian, China). DMEM and RPMI 1640 were purchased from Gibco BRL (Gaithersburg, USA). Fetal bovine serum was obtained from Gemini (California, USA). Penicillin and streptomycin were purchased from Melonepharma Co. Ltd. (Dalian, China). MCF-7 cells and MCF-7/ADR were provided by the cell bank of Chinese Academy of Sciences (Beijing, China).

2.2. Synthesis and characterization of B-TPP

The TPP^+ moiety was linked to Brij 98 via an esterified linker. In brief, TPP (1 mmol), EDCI (2.5 mmol), HOBT (2.5 mmol) and DMAP (6.5 mmol) were co-dissolved in DMSO (12 ml). Then 3-ml of Brij 98 solution (0.2 mmol in DMSO) was added to the mixture, which was stirred under nitrogen protection for 24 h at room temperature. The crude product was transferred to re-generated cellulose dialysis tubing (molecular weight cut-off point, MWCO 1000 Da) against distilled water for 48 h, followed by membrane filtration (0.45 μm). The lyophilized power was obtained for subsequent preparation of NCs. TPP^+-modified Brij 98 (B-TPP) was identified and characterized using nuclear magnetic resonance spectroscopy (400 MHz ^1H NMR, Bruker Corporation, Switzerland) and a Fourier transform infrared spectrometer (FTIR, Bruker Corporation, Switzerland).

2.3. Preparation and characterization of non-targeted and targeted PTX NCs

The PTX NCs were prepared as previously reported [22]. Briefly, PTX and Brij 98 were dissolved in ethanol at mass ratios of 1: 5 for non-targeted PTX NCs (named 0%B-TPP/PTX NCs). For targeted PTX NCs, 30% and 50% (mole present) of Brij 98 were replaced with B-TPP (named 30%B-TPP/PTX NCs and 50%B-TPP/PTX NCs, respectively). Afterwards, each mixture was co-precipitated by evaporating ethanol. Water was then allowed to add and hydrate the precipitate for 40 min. The resultant suspensions were sonicated for 10 min in a bath-type sonication to disperse the NCs. For the fluorescence-labeled NCs, coumarin-6 (co-precipitated with PTX at a mass ratio of 1:63) was integrated in the NCs in accordance with a similar process for preparing hybrid NCs.

The particle sizes, polydispersity indexes (PDI) and zeta potential values of PTX NCs were measured using a Malvern Zetasizer Nano ZS (Malvern Instruments Ltd., Malvern, Worcestershire, U.K.). The morphology of the obtained NCs was observed using a transmission electron microscope (TEM, JEM2100, JEOL, Japan).

2.4. Drug content assay and releasing behavior

The release behavior of PTX from the NCs was evaluated in the dialysis tubes (MWCO 10,000 Da) against PBS with pH 5.0, 6.5 or 7.4 with 0.5% SDS at 37 °C. At predetermined time intervals, 1 ml of the release medium was taken out and replaced

with fresh medium. The release medium was then analyzed by HPLC system with a UV detector (Hitachi Limited. Tokyo, Japan). The analysis was performed on an ODS column (Inertsil ODS-SP C18 column, 150 mm × 4.6 mm, 5.0 μm, GL Sciences Inc., Japan) at 30 °C. The mobile phase consisted of acetonitrile and water (45: 55, v/v). Flow rate was 1.0 ml/min and the detection wavelength was set at 227 nm.

2.5. Cell culture

The human breast adenocarcinoma cell lines MCF-7 and MCF-7/ADR were grown in DMEM medium and RPMI 1640 medium, respectively [23, 24]. The culture medium was supplemented with 10% fetal bovine serum (FBS) and antibiotics (1% penicillin-streptomycin, v/v). They were cultured in a humidified incubator with 5% CO_2 at 37 °C. The medium was replaced every other day.

2.6. Confocal microscopy

MCF-7 cells or MCF-7/ADR cells were seeded in 12-well plates with 1.5×10^5 cells per well and cultured for 24 h. For co-localization of the tested formulations and mitochondria, the cells were treated with coumarin-6-labeled 0%B-TPP/PTX NCs, 30%B-TPP/PTX NCs or 50%B-TPP/PTX NCs for 1, 4 or 12 h. Then the cells were washed with PBS and incubated with Mitotracker Red (35 nM) for 30 min. After staining, the cells were washed with PBS three times and fixed with 4% paraformaldehyde for 15 min at 37 °C. The cells were observed using a confocal C2-si laser scanning microscope (CLSM, Nikon C2 Plus, Japan). Images were then analyzed by Image-Pro Plus and the Pearson's correlation coefficient (R) was used to evaluate mitochondrial co-localization.

2.7. Cytotoxicity

MCF-7 cells or MCF-7/ADR cells were seeded at a density of 3000 cells/well into 96-well culture plates and cultured for 24 h under 5% CO_2 at 37 °C. The cells were then treated with various concentrations of the tested formulations. After incubated for another 24 h, the cells were washed with PBS and 10 μl of MTT solution (0.5 mg/ml in PBS solution) was added into each well. After 4 h, the supernatant in each well was removed and 150 μl of DMSO was added to dissolve the formed violet crystals. The UV absorbance at 570 nm was recorded using an ELISA microplate reader (Thermo Scientific Varioskan Flash, USA). The relative cell viability was normalized to that of untreated MCF-7 or MCF-7/ADR cells in the complete culture media. The experiments were repeated 3 times for statistical analysis.

2.8. Mitochondrial membrane potential

MCF-7 and MCF-7/ADR cells were seeded in a 96-well plates with 1×10^4 cells each well. After incubated for 24 h, the cells were treated with 0%B-TPP/PTX NCs, 30%B-TPP/PTX NCs, 50%B-TPP/PTX NCs and free PTX (at the equal dose of 0.5 μg/ml for MCF-7 cells and 5 μg/ml for MCF-7/ADR cells) for another 24 h. The cells were then washed with PBS, and TMRE (200 nM) was added into each well cultured for an additional 20 min. After washing twice with cold PBS, the fluorescence intensity of TMRE was measured by a microplate reader at the wavelength of Ex/Em = 547/575 nm. The MCF-7 or MCF-7/ADR cells were treated with FCCP (uncoupler, 20 μM) as the positive control.

2.9. Growing of MCF-7 and MCF-7/ADR multicellular spheroids (MCs)

3D MCF-7 and MCF-7/ADR MCs were produced using the classical hanging-drop method [25]. Briefly, the single-cell suspensions were adjusted to the appropriate concentration using culture media and mixed with methyl cellulose (0.48%, w/v) at the volume ratio of 1:1. After homogeneous mixing, 15 μl of the cell suspension was pipetted onto the lid of a U-bottomed 96-well plate, and then the lid was inverted. After sedimentation for 24 h, the plates were centrifuged at 1000 *g* for 5 min, followed by incubation at 37 °C with 5% CO_2 for 3 d.

2.10. Imaging of PTX NCs distribution in MCF-7 MCs

For imaging the PTX NCs distribution, the 3-d MCF-7 MCs were exposed to coumarin-6-labeled non-targeted and targeted PTX NCs at equivalent fluorescence intensity. After co-incubation for 2 h, the treated MCs were washed with PBS before imaging. The MCF-7 MCs were observed using a confocal laser scanning microscope.

2.11. MCF-7 and MCF-7/ADR MCs growth inhibition

The anticancer effect of NCs was finally analyzed via a growth inhibition assay on MCF-7 and MCF-7/ADR MCs. The MCs were incubated with non-targeted, targeted PTX NCs or free PTX for 5 d, respectively. The morphology of the treated MCs was observed using an inverted fluorescence microscope (Olympus IX71, Japan) and the diameters of the MCs were measured every other day as an indication of MCs proliferation evaluation. The untreated MCs were used as controls.

2.12. Statistical analysis

The data from all experiments in the present study were expressed as the mean ± standard deviation (SD). Statistical analysis was conducted using the two-tailed unpaired t test for the comparison between two groups. A one-way ANOVA were performed for three or more experimental groups followed by the Tukey multiple comparison tests using Graph Pad Prism. $P < 0.05$ were considered statistically significant (*), $P < 0.01$ were considered highly significant (**) and $P < 0.001$ were considered extremely significant (***), respectively.

3. Results and discussion

3.1. Synthesis and characterization of B-TPP

As depicted in Scheme 1, carbodiimide chemistry was used to covalently conjugate TPP to Brij 98. The formation of the conjugate was confirmed using FT-IR (Fig. 1A) and ^{1}H NMR (Fig. 1B) spectroscopy. The comparison of the FT-IR spectra for TPP, Brij 98 and B-TPP conjugate showed specific peaks at

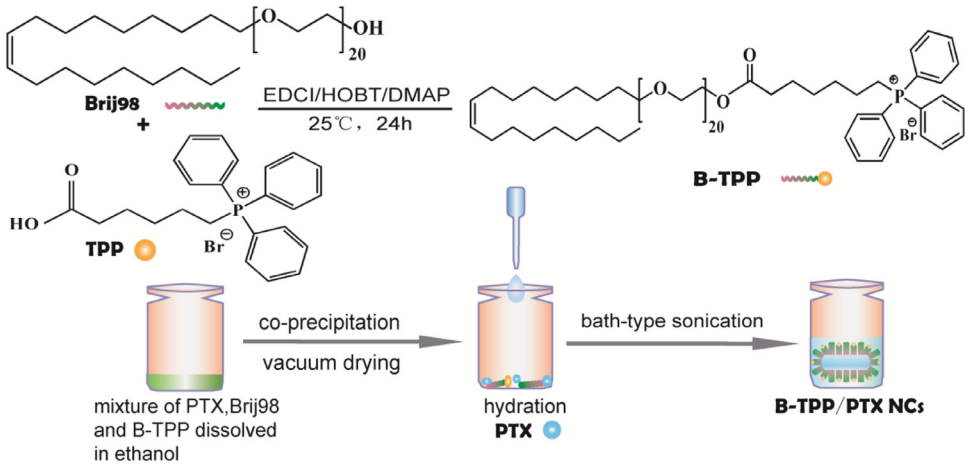

Scheme 1. – Schematic diagram of (A) synthesis of B-TPP and the preparation of paclitaxel nanocrystals (PTX NCs). B-TPP was synthesized through esterification reaction. Then B-TPP/PTX NCs was prepared for mitochondrial targeting strategy.

Table 1. – Particle sizes and zeta potential of PTX NCs as determined via DLS ($n = 3$).

	Particle size (nm)	PDI[a]	Zeta potential (mV)
0% B-TPP/PTX NCs	187.6 ± 1.210	0.216 ± 0.017	−6.80 ± 0.14
30% B-TPP/PTX NCs	199.8 ± 2.816	0.211 ± 0.006	20.17 ± 0.04
50% B-TPP/PTX NCs	176.1 ± 11.67	0.159 ± 0.002	27.33 ± 0.04

[a] PDI, polydispersity index.

1705, 1630–1640 and 750–690 cm^{-1}, corresponding to the carbonyl (C=O) of TPP, the double bond (C=C) of Brij 98 and the phenyl ring (–ArH) of TPP, respectively. The characteristic peak of the carbonyl bond (C=O) in B-TPP shifted from 1705 cm^{-1} to 1730 cm^{-1} coupled with a strong typical peak of C–O–C asymmetrical stretching peak at 1112.4 cm^{-1}, indicating that Brij 98 and TPP were linked by an ester bond. As shown in the ^1H NMR spectrum, the appearance of signals at 7.7–7.9 ppm and ~3.5 ppm in B-TPP were attributed to the proton in the phenyl ring in TPP and PEG in Brij 98 respectively, indicating the formation of a conjugate. Furthermore, the conjugation efficiency was estimated at ~70% by comparing the integrals of aromatic signal at 7.7–7.9 ppm.

3.2. *Preparation and characterization of PTX NCs*

PTX NCs were prepared using Brij 98 or B-TPP as the stabilizers. Table 1 lists the average particle sizes, polydispersity index (PDI) and zeta potential values of 0%B-TPP/PTX NCs, 30%B-TPP/PTX NCs and 50%B-TPP/PTX NCs determined by dynamic light scattering analysis. The mean particle sizes of various PTX NCs ranged from 176.1 to 199.8 nm with narrow size distributions (PDI: ~0.2). After TPP^+ modification, the zeta potential of PTX NCs shifted from −6.80 ± 0.14 mV (0%B-TPP/PTX NCs) to 20.14 ± 0.04 mV (30%B-TPP/PTX NCs) and 27.33 ± 0.04 mV (50%B-TPP/PTX NCs), respectively. Fig. 2 illustrates the morphology of PTX NCs observed by TEM. All resulting NCs exhibited a rod-shape with mean length of ~380 nm and mean diameter of ~40 nm.

3.3. *In vitro releasing behavior*

Fig. 3 illustrates the releasing behavior of free PTX and PTX NCs. It was shown that ~85% of PTX released from PTX solution within 36 h in varied pH medium, whereas the PTX NCs demonstrated sustained release profiles with zero-order kinetics. Specially, 0%B-TPP/PTX NCs resulted in 56.9% ± 1.6% released at pH 5.0, 49.1% ± 3.5% released at pH 6.5 and 39.7% ± 1.9% released at pH 7.4 in 36 h, indicating acidic condition favored the release of PTX from NCs. While compared with 0%B-TPP/PTX NCs, TPP^+-modified PTX NCs promoted the release of PTX as the evidence of ~10% increased cumulative release observed in the corresponding medium.

3.4. *Mitochondrial co-localization*

Before the co-localization evaluation, free coumarin-6 at the equivalent labeled amount was first incubated with cells. No intracellular fluorescence signal was observed, indicating no interference in the obtained images (Fig. S1). To assess the targeted ability of the TPP^+-modified PTX NCs, we used a commercial dye, Mitotracker Red, to stain the mitochondria in MCF-7 or MCF-7/ADR cells for the evaluation. Fig. 4 shows the images of MCF-7 cells incubated with the tested formulations at varying TPP^+ densities. In the merged images, the significant yellow overlay between TPP^+-modified NCs (green fluorescence) and Mitotracker Red (red fluorescence) was found in the TPP^+-modified formulations. The Person's correlation coefficient (R) was then calculated to quantitatively compare the mitochondria-targeted ability after 4 h of incubation. The R values of mitochondria with PTX NCs at 30% and 50% TPP^+-modified density were 0.594 and 0.545, respectively, which were much higher than that from the system composed of the unmodified group ($R < 0.1$). For PTX-resistant cells, TPP^+-modified PTX NCs also demonstrated mitochondrial targeting ability. As

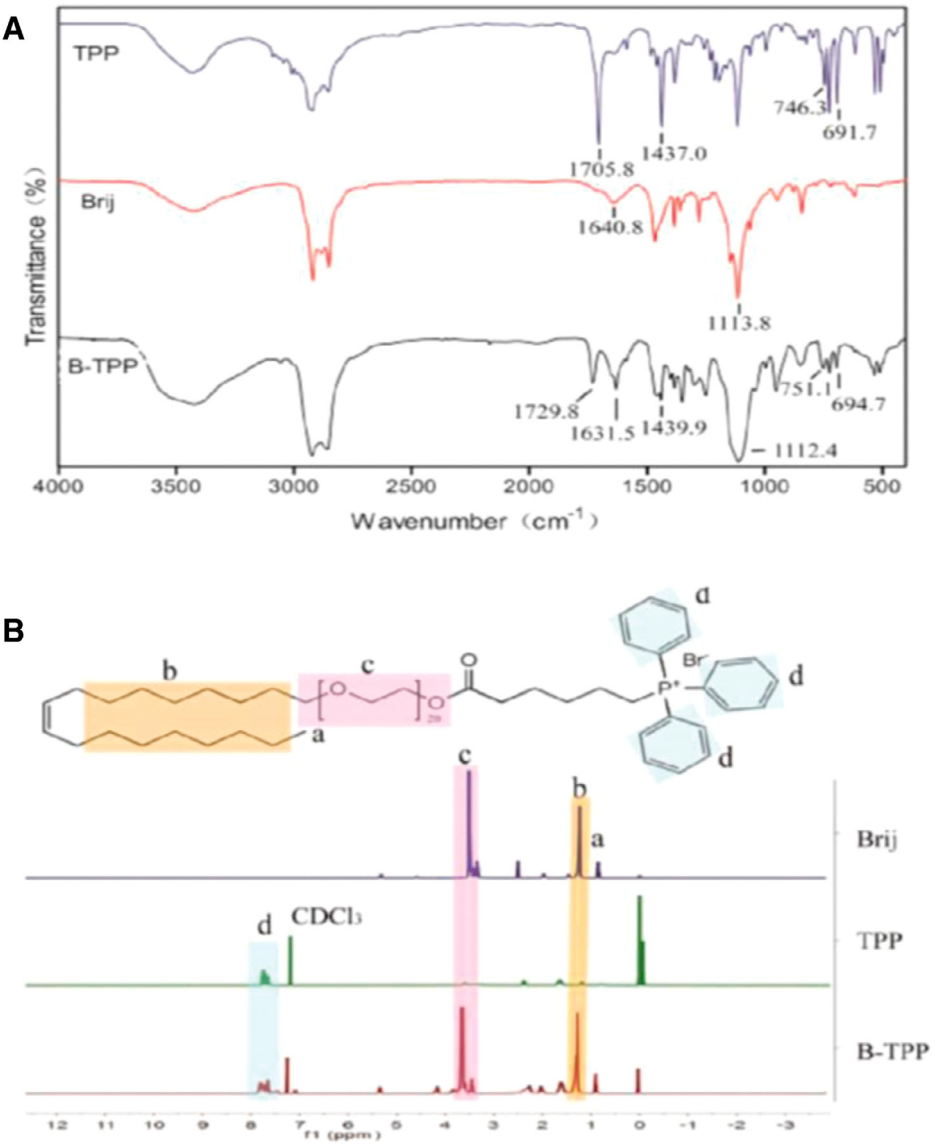

Fig. 1 – Spectrum of (A) FIIR and (B) 1H-NMR for Brij 98, TPP and B-TPP. (A) FTIR spectrum of TPP (KBr, cm^{-1}): υ(C=O) 1705.8, υ(P–Ar) 1437.0, γ(Ar–H) 746.3 and 691.7; FTIR spectrum of Brij 98, (KBr, cm^{-1}): υ(C=C) 1640.8, υ(C–O–C) 1113.8; FTIR spectrum of B-TPP, (KBr, cm^{-1}): υ(C=O) 1729.0, υ(C=C) 1631.5, υ(P–Ar) 1439.9, υ(C–O–C) 1112.4, γ(Ar–H) 751.1 and 694.7. (B) 1HNMR (CDCl3, 400 MHz): δ 7.9–7.7(15H, m, Ar–H), ~3.5 (82H, t, O–CH_2), 0.88(3H, t,-CH_3) ppm.

shown in Fig. 5, *R* values of 30%B-TPP/PTX NCs and 50%B-TPP/PTX NCs were 0.866 and 0.833 after incubated for 12 h whereas that of 0%B-TPP/PTX NCs was 0.681. These results confirmed that modification with TPP^+ on the surface of PTX NCs possessed the capacity of mitochondrial specific distribution.

Normally, TPP^+ and other TPP^+ derivatives are currently being developed to be used as mitochondria-targeted agents, exhibiting selectively targeting cancer cells due to the specific features of tumor mitochondria different from those of other cellular compartments and normal mitochondria. Notably, a stronger negative MMP of −150 to −180 mV is observed in carcinoma cells to fit with highly up-regulated ATP synthesis, making TPP-based cations preferentially accumulated in mitochondria [26]. Several studies have utilized the TPP^+moiety to modify nanoparticles for the mitochondrial delivery of PTX. For example, PTX loaded TPP^+-modified liposomes exhibited higher efficiency in cytotoxic effects against Hela cells *in vitro* as well as tumor growth inhibitory activity against breast cancer xenografts in mice *in vivo* [27].

In addition, after incubation with various PTX NCs for 1 h, intracellular TPP^+-modified PTX NCs demonstrated diffuse as well as punctuate fluorescence, but only punctuate fluorescence was observed for unmodified PTX NCs. Furthermore, the number of punctuate dots in MCF-7 cells decreased after treating with TPP^+-modified PTX NCs for 4 h. Specifically, punctuate fluorescence was regarded as an indication of endosomal localization, implying an endocytosis-mediated uptake mechanism. As previous reports suggested, positively charged nanoparticles were predominantly

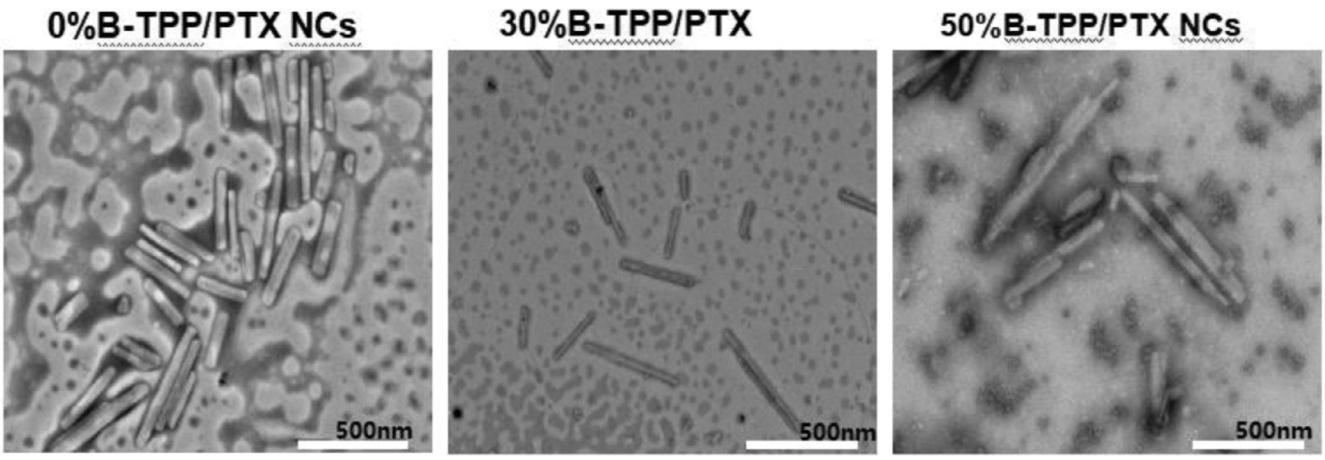

Fig. 2 – The TEM images of 0% B-TPP/PTX NCs, 30%B-TPP/PTX NCs and 50% B-TPP/PTX NCs. Scale bars = 500 nm.

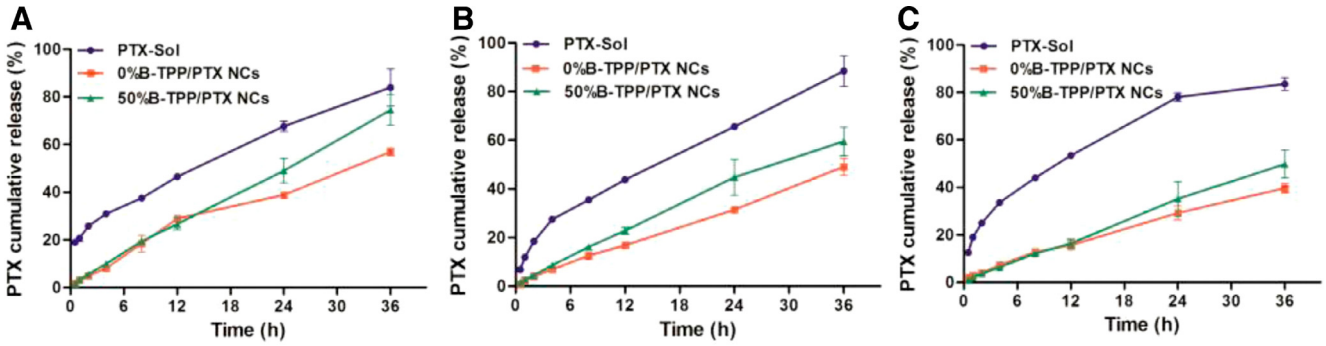

Fig. 3 – Release kinetics of 0%B-TPP/PTC NCs, 50% B-TPP/PTC NCs and free PTX (PTX-Sol) in the (A) PBS at pH 5.0, (B) PBS at pH 6.5 and (C) PBS at pH 7.4.

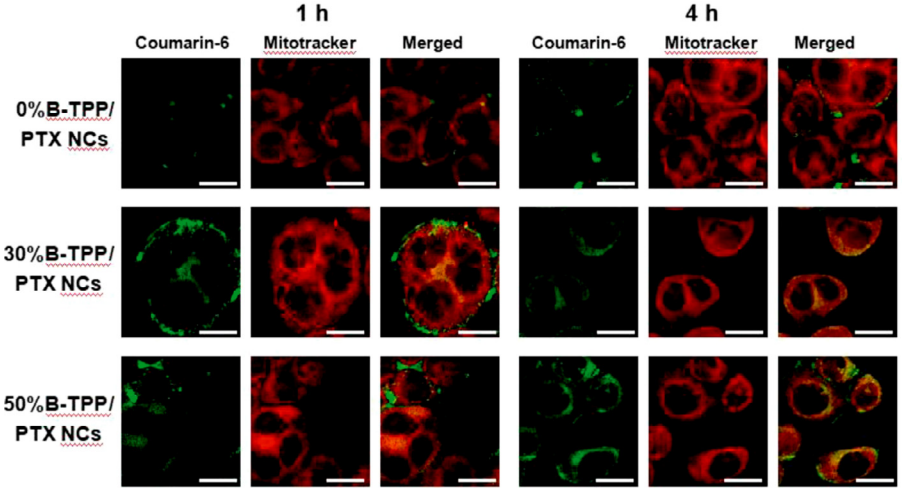

Fig. 4 – Time-dependent cellular uptake and co-localization of coumarin-6-labeled PTX NCs on MCF-7 cells. MCF-7 cells were treated with mitochondria-targeted or non-targeted PTX NCs for 1 h and 4 h, respectively. Yellow spots in the merged picture denoted the co-localization of the PTX NCs (labeled with coumarin-6, green fluorescence) with mitochondrial compartments (stained with Mitotracker Red, red fluorescence). Scale bar = 10 μm.

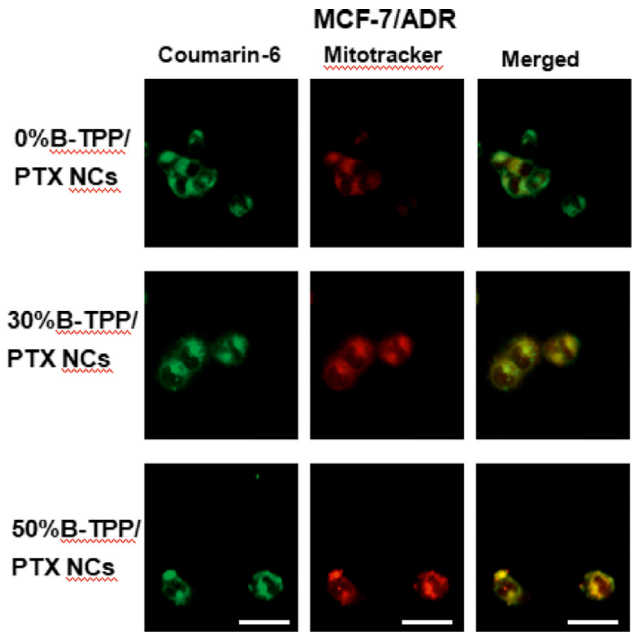

Fig. 5 – Co-localization of coumarin-6-labeled PTX NCs on MCF-7/ADR cells. Cells were treated with mitochondria-targeted or non-targeted PTX NCs for 12 h, respectively. Yellow spots in the merged picture denoted the co-localization of the PTX NCs (labeled with coumarin-6, green fluorescence) with mitochondrial compartments (stained with Mitotracker Red, red fluorescence). Scale bars = 15 μm.

internalized through clathrin-mediated endocytosis [28, 29]. Moreover, the escape of preparations from the endosome and lysosome is one of the crucial steps in delivering drugs into subcellular organelle. For mitochondria-targeted delivery, TPP^+-modified drug delivery system has widely displayed its capacity of endosomal and lysosomal escape [15, 30–32]. The buffering capacity of positively charged PEG, known as "proton sponges", probably accounts for the efficient endosomal escape of targeted preparations [33, 34].

3.5. *The cytotoxicity of non-targeted and targeted PTX NCs on MCF-7 cells*

The cytotoxicity of free PTX and various PTX NCs on MCF-7 cells was investigated by MTT assay (Fig. 6A). We concluded that both PTX NCs and free PTX inhibited the proliferation of MCF-7 cells in a concentration-dependent manner. As shown in Fig. 6A, MCF-7 cells demonstrated superior sensitivity against the PTX NCs over that of the free drug. Specially, the targeted PTX NCs exhibited higher inhibitory effects than did the non-targeted PTX NCs, except for the group treated with 0.025 μg/ml PTX NCs. Furthermore, no distinguishing inhibitory effects were observed between 30%B-TPP/PTX NCs and 50%B-TPP/PTX NCs at the investigated range of drugs but 0.01 μg/ml of PTX. To clarify the inhibitory effects of designed formulations, we also evaluated the cytotoxicity of blank stabilizer (Brij 98 or the mixture of Brij 98 and B-TPP) in the MCF-7 cells (Fig. S2). The results demonstrated that all the stabilizers exhibited much lower cytotoxicity than that of NCs at the corresponding concentration, excluding their potential inhibitory effects.

Previous reports suggested that PTX could inhibit the proliferation of cancer cells via the mitochondrial pathway

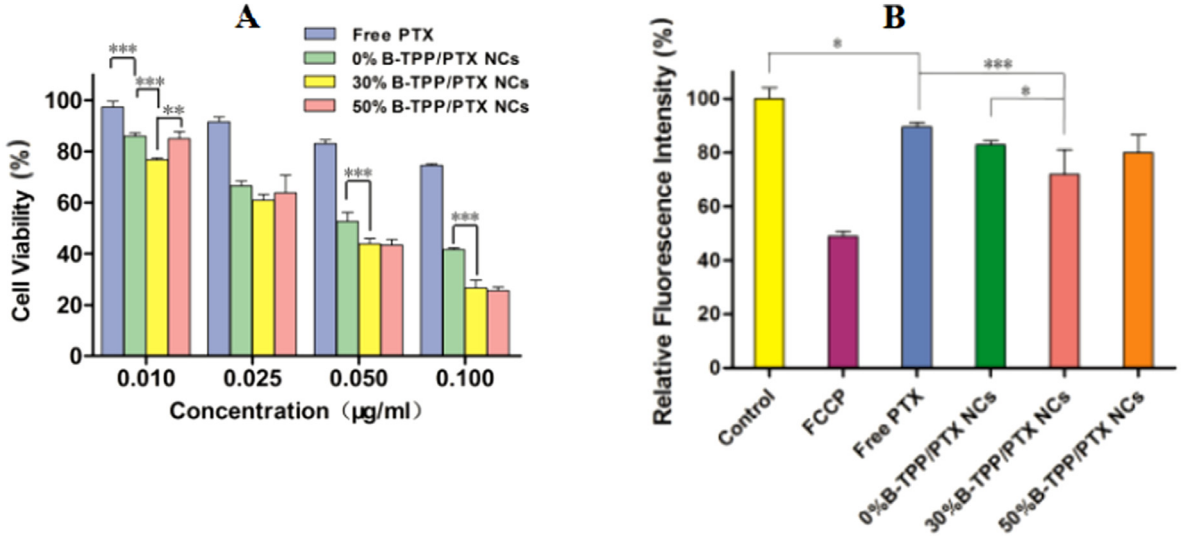

Fig. 6 – Cell viability of (A) MCF-7 cells treated with 0%B-TPP/PTX NCs, 30%B-TPP/PTX NCs, 50%B-TPP/PTX NCs and free PTX. Cell viability was assessed by MTT assay upon 24 h of incubation after being treated with various concentrations of non-targeted, targeted PTX NCs or free PTX for 4 h. (B) Mitochondrial membrane potential of MCF-7 cells treated with 0.05 μg/ml free PTX, 0%B-TPP/PTX NCs, 30%B-TPP/PTX NCs and 50% B-TPP/PTX NCs, respectively. MCF-7 cells were treated with 20 μM FCCP as the positive control. ($n = 3$).

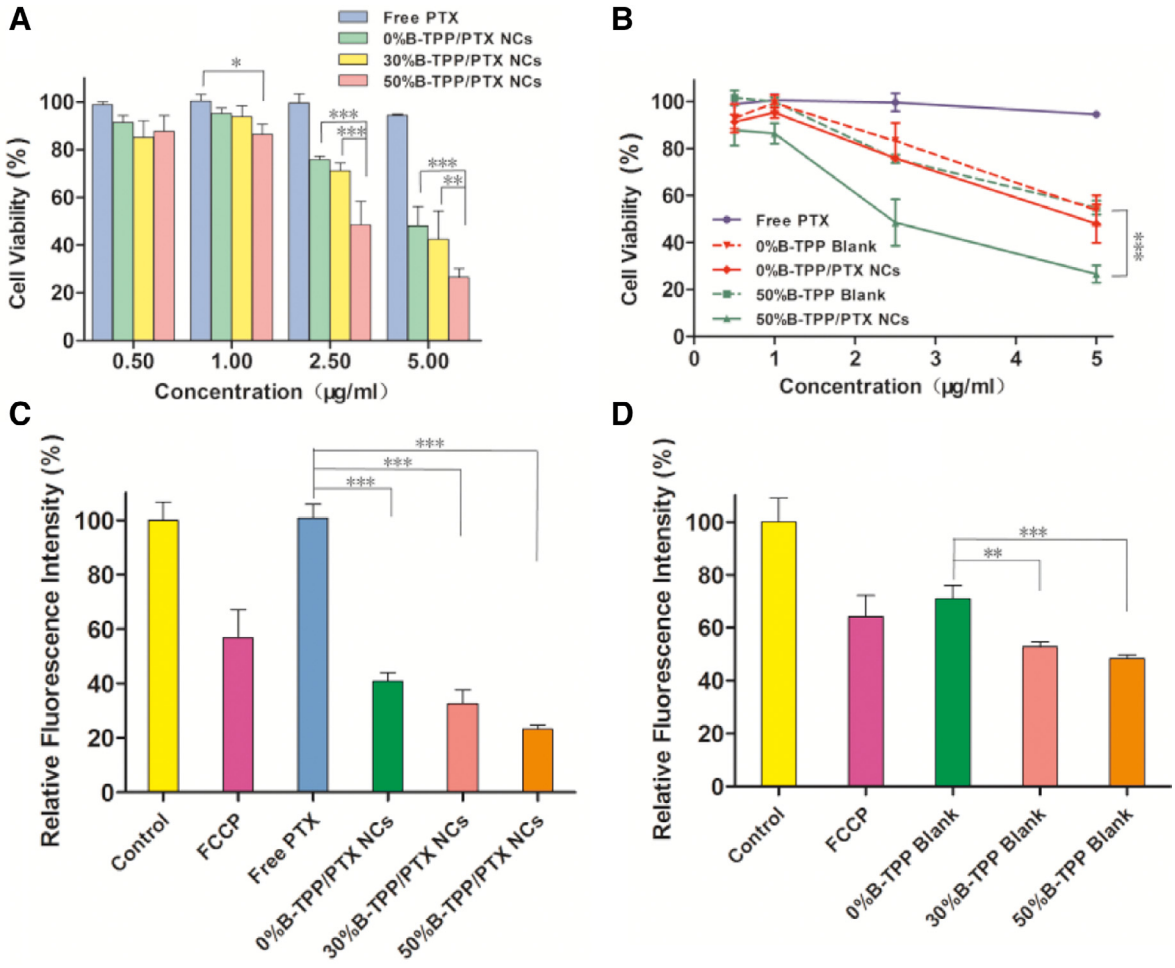

Fig. 7 – Cell viability of (A) MCF-7/ADR cells treated with 0%B-TPP/PTX NCs, 30%B-TPP/PTX NCs, 50%B-TPP/PTX NCs and free PTX. Cell viability was assessed by MTT assay upon 24 h of incubation after being treated with various concentrations of non-targeted, targeted PTX NCs or free PTX for 4 h (B) Cell viability of MCF-7/ADR cells treated with various concentrations of free PTX, 0%B-TPP/PTX NCs, 50%B-TPP/PTX NCs and corresponding blank stabilizers. The concentration denotes the mass concentration of PTX in the culture media. Mitochondrial membrane potential of MCF-7/ADR cells treated with (C) various formulations containing PTX and (D) corresponding blank stabilizers. MCF-7/ADR cells were treated with 20 μM FCCP as the positive control ($n = 3$).

[35–37]. Here, we evaluated the mitochondrial membrane potential (MMP) of MCF-7 cells since MMP is regarded as an early signal of mitochondria-triggered apoptosis. TMRE was used as indicator of MMP and the method was validated by FCCP, an uncoupler to dissipate MMP. After treating MCF-7 cells with PTX containing formulations, we demonstrated that the MMP significantly decreased compared to that of the mock-treated group (Fig. 6B). Meanwhile, the highest inhibition of MMP was observed in the treatment with 30%B-TPP/PTX (28.1% ± 9.2% of the mock treated group), followed by 50%B-TPP/PTX NCs (20.1% ± 6.6%), 0% B-TPP/PTX NCs (17.2% ± 1.5%) and free PTX (10.5% ± 1.8%).

3.6. *The cytotoxicity of non-targeted and targeted PTX NCs on MCF-7/ADR cells*

To investigate the therapeutic potential against MCF/ADR cells, the cytotoxicity of 0%B-TPP/PTX NCs, 30%B-TPP/PTX NCs, 50%B-TPP/PTX NCs and free PTX were assessed. As presented in Fig. 7A, free PTX barely inhibited the proliferation of MCF-7/ADR cells even when 5 μg/ml free PTX was used. This lack of inhibition might be because PTX was pumped out via the overexpression of the efflux protein on the cell membrane leading to intracellular drug concentration less than the threshold value of cell lethal dose [38]. In contrast, MCF-7/ADR cells showed dose-dependent sensitivities against the designed formulations. Among all the tested PTX NCs, 50%B-TPP/PTX NCs showed the highest inhibitory effect, provided that the concentration of PTX exceeded 1 μg/ml. Notably, the mortality rate of MCF-7/ADR cells was 73.5% ± 3.7% upon 50%B-TPP/PTX NCs at the dose of 5 μg/ml PTX, which was significantly higher than 0%B-TPP/PTX NCs (52.0% ± 8.2%) and 30%B-TPP/PTX NCs (57.5% ± 11.8%). To clarify the possible reason for the discrepant therapeutic potential, the antiproliferative effect of the blank stabilizer on MCF-7/ADR cells was further assessed. It clearly proved that the toxicity of

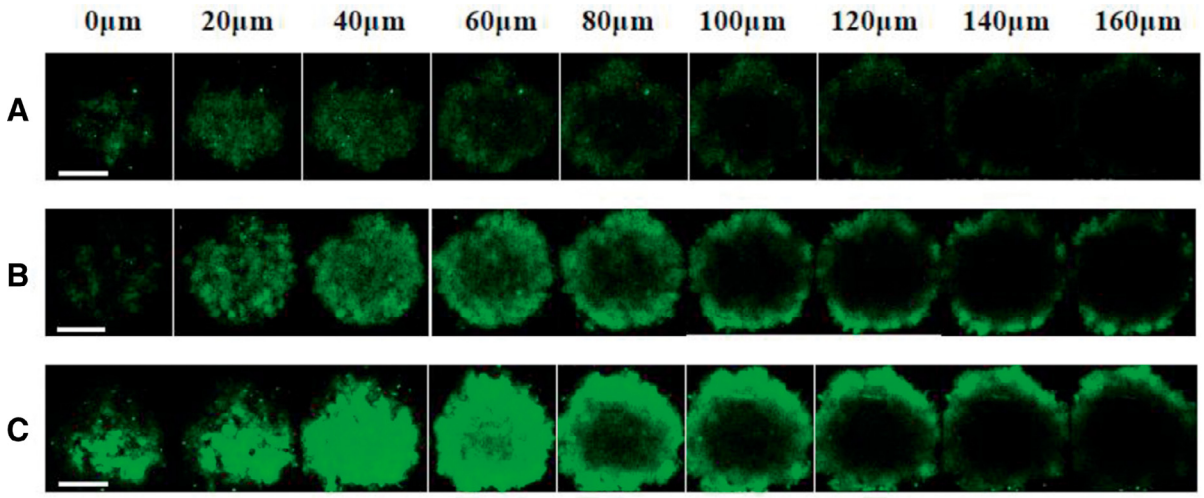

Fig. 8 – Representative Z-stack images of MCs after treatment with equivalent coumarin-6 labeled (A) 0%B-TPP/PTX NCs, (B) 30%B-TPP/PTX NCs and (C) 50%B-TPP/PTX NCs, respectively, for 2 h were obtained from starting at the top of the spheroid in 20 μm intervals. Scale bars = 200 μm.

0%B-TPP/PTX NCs was no significant difference compared to that of the unloaded NCs (Fig. 7B). Conversely, 50%B-TPP/PTX NCs showed more potent toxicity than that of the blank stabilizer, indicating the crucial effect of mitochondrial accumulation PTX against the resistant cell line. Meanwhile, the cytotoxicity of the tested formulations exhibited a TPP^+ density-dependent effect, which was quite different in the non-resistant cells. For comparison, we also evaluated the MMP of MCF-7/ADR cells after various treatments and the results are shown in Fig. 7C and D. Compared to that of free PTX (100.7% ± 5.1% of the mock treated group) and non-targeted PTX loaded NCs (40.7% ± 3.2%), more significant decreases in MMP can be observed in the group of targeted NCs (23.2% ± 1.6% for the 50%B-TPP/PTX NCs treated group and 32.5% ± 5.2% for 30%B-TPP/PTX NCs treated group). The dissipation of MMP could indicate the alteration of dysfunctional mitochondria caused by the mitochondria-targeted delivery of PTX. After treating with various blank stabilizers, different levels of decrease in MMP of MCF-7/ADR cells were also observed. Compared with 0%B-TPP Blank (70.9% ± 4.9%), targeted stabilizers (52.7% ± 1.9% for the 30%B-TPP Blank group and 48.3% ± 1.3% for 50%B-TPP Blank group) demonstrated more significant effect on mitochondrial damage. The mitochondrial uncoupling effect of TPP^+ was deemed to account for the results.

The present study aimed to evaluate the synergistic effect of novel drug delivery system in overcoming MDR of PTX. As demonstrated in Figs. 6 and 7, non-targeted loaded PTX NCs showed improved inhibition of proliferation in both of MCF cells and MCF/ADR cells compares to that of free drug, which was consistent with the previous reports. Here, we identified Brij 98 as the lethal source of non-targeted NCs against MCF/ADR cells, as the evidence of no significant difference in cytotoxicity observed between the blank stabilizer and non-targeted PTX NCs (Fig. 7B). Conversely, the enhanced cytotoxicity of targeted PTX NCs against MCF/ADR cells was in a special manner (Fig. 7B), which differed significantly from the mitochondria-targeted blank stabilizer. It indicated that the mitochondrial delivery of PTX might mainly account for their therapeutic sensitivity to those cells. Mitochondria were identified as the primary targets of TPP^+-modified formulations, being converted to pro-death organelles through inhibition of mitochondrial respiration and ATP synthesis. More pronounced downstream MMP and mitochondrial apoptotic cell death were activated by the treatment with TPP^+-modified PTX NCs, attributing to its superior sensitivity in MCF/ADR cells.

In addition, TPP^+ moiety using for mitochondrial drug delivery was found to demonstrate specific cytotoxicity. For example, an approach using TPP^+-modified liposomes for PTX was developed to mitochondrial drug delivery and was reported to result in enhanced cytotoxicity in a PTX-resistant cell line. However, the enhanced cytotoxicity was revealed to be partly resulting from the specific toxicity of STPP toward the resistant cell line [18]. Several derivatives of alkyl-TPP^+ were reported to selectively inhibit the proliferation of cancer cells due to their effect as potential uncouplers, which were proposed to dissipate MMP and then decrease ATP production [39, 40]. These effects on mitochondrial function were known to correlate with the increasing hydrophobicity of TPP^+ derivatives with increasing alkyl chain length. Several attempts were made to covalently conjugate PEG to the TPP^+ moiety in order to decrease the related toxicity from formulations. For example, Bielski et al. observed decreased toxicity of the TPP^+-modified poly-(amidoamine) (PAMAM) with PEG as a linker between the dendrimer and TPP^+, while the mitochondrial targeting ability of the nanocarriers was not affected [41]. In the present study, TPP^+ was utilized to conjugate Brij 98, a non-ionic surfactant with a PEG motif, resulting in efficient mitochondrial delivery (Figs. 4 and 5) and decreased the toxicity stemming from TPP^+ (Fig. 7).

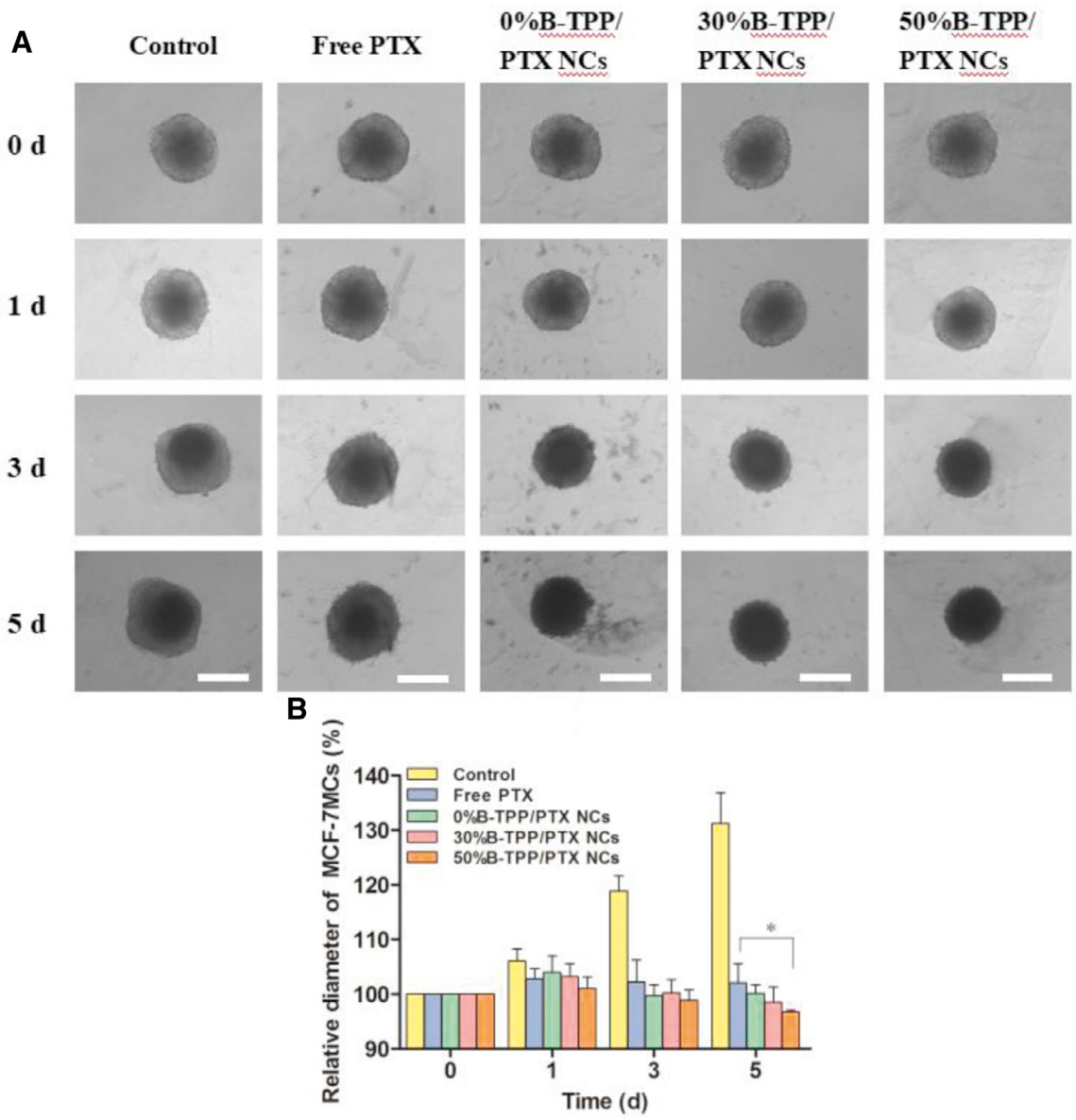

Fig. 9 – (A) Morphology of MCF-7/ADR MCs treated with targeted, non-targeted PTX NCs and free PTX at the equal dose of 0.5 μg/ml, Scale bars = 500 μm. (B) Growth tendency of MCF-7/ADR MCs after co-incubated with free PTX, 0%B-TPP/PTX NCs, 30%B-TPP/PTX NCs or 50%B-TPP/PTX NCs for 5 d, respectively. Medium treated MCs were used as control. Relative diameter of MCF-7/ADR MCs (%) was calculated according to the ratio of intraday diameter of MCs and its initial diameter (0 d).

3.7. Penetration and growth inhibition evaluation in 3D MCs

The tumor penetration efficiency of the tested formulations was analyzed using confocal microscopy by assessing the fluorescence at different focal planes in the spheroid (Z slices) represented in Fig. 8. As depicted in Fig. 8, the depth of green fluorescence from the periphery to the inner in MCs were ~110 and ~140 μm after the treatment with the 30%B-TPP/PTX NCs and 50%B-TPP/PTX NCs for 2 h, respectively, while only ~80 μm was observed in the treatment of the 0%B-TPP/PTX NCs. The result indicated the superior ability of targeted NCs to penetrate deeper tumor mass when compared to that of non-targeted NCs.

To further investigate the anti-tumor effect, we cultured MCF-7 MCs and MCF-7/ADR MCs with medium containing free PTX, 0%B-TPP/PTX NCs, 30%B-TPP/PTX NCs or 50%B-TPP/PTX NCs at the equivalent dose (1 μg/ml for MCF-7 MCs and 5 μg/ml for MCF-7/ADR MCs) for 5 d, with mock-treated MCs used as control. The spheroids were observed every other day for change in morphology. Images were captured using an inverted microscope to further determine the diameter of the MCs. As shown in Fig. 9A, untreated MCF-7/ADR MCs grew up obviously with a significant increase in the spheroidal diameter (~532.7 ± 32.7 μm and ~633.1 ± 17.8 μm on day 0 and day 5, respectively) (Fig. 9B). In the contrast, more significant inhibition effect in spheroidal diameters and morphology of MCF-7/ADR MCs were observed in PTX

NCs treated groups with incubation time going. As can be seen in Fig. 9B, 50%B-TPP/PTX treated spheroids showed suppressed growth as indicated by the reduced spheroidal diameter of ~416.0 ± 30.1 μm on day 5 compared to the diameter on day 0 (~502.1 ± 36.7 μm). As for free PTX treated MCs, a slight inhibitory effect was observed after 5-day culture, with the diameter of MCs changing from ~533.8 ± 2.8 μm to ~580.1 ± 24.9 μm. Moreover, 0%B-TPP/PTX NCs had a significant spheroidal growth inhibitory effect (spheroidal diameter of ~516.8 ± 5.7 μm on day 0 and ~439.9 ± 2.3 μm on day 5). However, a reduction in spheroidal size was evident following 50%B-TPP/PTX treatment. Various formulations treated MCF-7 MCs demonstrated similar growth inhibition effect (Fig. S3). Targeted PTX NCs exhibited more potent suppression of MCs growth compared to non-targeted PTX NCs and free PTX.

The study revealed that the targeted NCs resulted in the deeper distribution of MCs compared with non-targeted formulation. When an equal quantity of PTX was administered to MCF-7/ADR or MCF-7 MCs via the targeted and non-targeted NCs, a mild enhanced inhibition was observed for the targeted NCs treatment. The introduction of mitochondria-targeted moiety could account for the enhancement in MDR reversal behavior. Considering the stability issue of the designed NCs upon heavily dilution by systemic administration, intra-tumoral injection was thought to rational for the superior efficacy. The sustained releasing behavior, endocytosis-mediated rapid uptake and deeper distribution of targeted NCs could ensure that maximum of PTX co-localize into mitochondria. In future studies, the detailed *in vivo* evaluation of these formulations in experimental tumor-bearing animals must be carried out.

4. Conclusion

In the present study, a mitochondria-targeted B-TPP was synthesized and modified onto PTX NCs to overcome drug-resistant cancer. The B-TPP modified PTX NCs exhibited preferential accumulation in mitochondria and thus enhanced the cytotoxic effect in PTX-sensitive and PTX-insensitive MCF-7 cell lines. The mechanism in their improved cytotoxicity stemmed from the cell apoptosis via mitochondrial path with dissipated MMP as early indicators. Using MCF-7 MCs mimicking solid tumors *in vitro*, the TPP^+-modified PTX NCs demonstrated deeper penetration and more potent growth inhibition than did non-targeted PTX NCs. Our work identified TPP^+-modified NCs as a new strategy for overcoming MDR via high drug loading of PTX with mitochondrial delivery to specifically induce mitochondrial apoptosis. Subsequently, *in vivo* experiments will be required to evaluate the potential clinical application.

Conflict of interest

The authors report no conflicts of interest. The authors alone are responsible for the content and writing of this article.

Supplementary materials

Supplementary material associated with this article can be found, in the online version, at doi:10.1016/j.ajps.2018.06.006.

REFERENCES

[1] Cao JH, He JL, Xu JY, et al. Polymeric prodrugs conjugated with reduction-sensitive dextran-camptothecin and pH-responsive dextran-doxorubicin: an effective combinatorial drug delivery platform for cancer therapy. Polym Chem 2016;7(25):4198–212.

[2] Liu Y, Sun J, Lian H, Cao W, Wang Y, He Z. Folate and CD44 receptors dual-targeting hydrophobized hyaluronic acid paclitaxel-loaded polymeric micelles for overcoming multidrug resistance and improving tumor distribution. J Pharm Sci 2014;103(5):1538–47.

[3] Bao Y, Guo Y, Zhuang X, et al. D-alpha-tocopherol polyethylene glycol succinate-based redox-sensitive paclitaxel prodrug for overcoming multidrug resistance in cancer cells. Mol Pharm 2014;11(9):3196–209.

[4] Zhang J, Wang L, Chan HF, et al. Co-delivery of paclitaxel and tetrandrine via iRGD peptide conjugated lipid-polymer hybrid nanoparticles overcome multidrug resistance in cancer cells. Sci Rep 2017;7:46057.

[5] Gao L, Liu G, Ma J, et al. Paclitaxel nanosuspension coated with P-gp inhibitory surfactants: II. Ability to reverse the drug-resistance of H460 human lung cancer cells. Colloids Surf B Biointerfaces 2014;117:122–7.

[6] Baek JS, Cho CW. Controlled release and reversal of multidrug resistance by co-encapsulation of paclitaxel and verapamil in solid lipid nanoparticles. Int J Pharm 2015;478(2):617–24.

[7] Xu Y, Asghar S, Gao S, et al. Polysaccharide-based nanoparticles for co-loading mitoxantrone and verapamil to overcome multidrug resistance in breast tumor. Int J Nanomed 2017;12:7337–50.

[8] Bhagya N, Chandrashekar KR. Tetrandrine and cancer – an overview on the molecular approach. Biomed Pharmacother 2018;97:624–32.

[9] Bu H, He X, Zhang Z, Yin Q, Yu H, Li Y. A TPGS-incorporating nanoemulsion of paclitaxel circumvents drug resistance in breast cancer. Int J Pharm 2014;471(1–2):206–13.

[10] Assanhou AG, Li W, Zhang L, et al. Reversal of multidrug resistance by co-delivery of paclitaxel and lonidamine using a TPGS and hyaluronic acid dual-functionalized liposome for cancer treatment. Biomaterials 2015;73:284–95.

[11] Liu H, Ma Y, Liu D, Fallon JK, Liu F. The effect of surfactant on paclitaxel nanocrystals: an *in vitro* and *in vivo* study. JBN 2016;12(1):147–53.

[12] Tang J, Wang Y, Wang D, et al. Key structure of Brij for overcoming multidrug resistance in cancer. Biomacromolecules 2013;14(2):424–30.

[13] Kalyanaraman B, Cheng G, Hardy M, et al. A review of the basics of mitochondrial bioenergetics, metabolism, and related signaling pathways in cancer cells: therapeutic targeting of tumor mitochondria with lipophilic cationic compounds. Redox Biol 2018;14:316–27.

[14] Zhou X, Chen R, Yu Z, et al. Dichloroacetate restores drug sensitivity in paclitaxel-resistant cells by inducing citric acid accumulation. Mol Cancer 2015;14(63):1–12.

[15] Zhang Y, Zhang C, Chen J, et al. Trackable mitochondria-targeting nanomicellar loaded with doxorubicin for overcoming drug resistance. ACS Appl Mater Interfaces 2017;9(30):25152–63.

[16] Qu Q, Ma X, Zhao Y. Targeted delivery of doxorubicin to mitochondria using mesoporous silica nanoparticle nanocarriers. Nanoscale 2015;7(40):16677–86.
[17] Prochazka L, Koudelka S, Dong LF, et al. Mitochondrial targeting overcomes ABCA1-dependent resistance of lung carcinoma to alpha-tocopheryl succinate. Apoptosis 2013;18(3):286–99.
[18] Solomon MA, Shah AA, D'Souza GG. *In vitro* assessment of the utility of stearyl triphenyl phosphonium modified liposomes in overcoming the resistance of ovarian carcinoma Ovcar-3 cells to paclitaxel. Mitochondrion 2013;13(5):464–72.
[19] Zhou J, Zhao WY, Ma X, et al. The anticancer efficacy of paclitaxel liposomes modified with mitochondrial targeting conjugate in resistant lung cancer. Biomaterials 2013;34(14):3626–38.
[20] Li WQ, Wang Z, Hao S, et al. Mitochondria-targeting polydopamine nanoparticles to deliver doxorubicin for overcoming drug resistance. ACS Appl Mater Interfaces 2017;9(20):16793–802.
[21] Han M, Vakili MR, Abyaneh HS, Molavi O, Lai R, Lavasanifar A. Mitochondrial delivery of doxorubicin via triphenylphosphine modification for overcoming drug resistance in MDA-MB-435/DOX cells. Mol Pharm 2014;11(8):2640–9.
[22] Liu F, Park JY, Zhang Y, et al. Targeted cancer therapy with novel high drug-loading nanocrystals. J Pharm Sci 2010;99(8):3542–51.
[23] Musacchio T, Toniutti M, Kautz R, Torchilin VP. 1H NMR detection of mobile lipids as a marker for apoptosis: the case of anticancer drug-loaded liposomes and polymeric micelles. Mol Pharm 2009;6(6):1876–82.
[24] Ji W, Wang B, Fan Q, Xu C, He Y, Chen Y. Chemosensitizing indomethacin-conjugated dextran-based micelles for effective delivery of paclitaxel in resistant breast cancer therapy. PLoS One 2017;12(7):1–12.
[25] Zhang W, Li C, Baguley BC, et al. Optimization of the formation of embedded multicellular spheroids of MCF-7 cells: how to reliably produce a biomimetic 3D model. Anal Biochem 2016;515:47–54.
[26] Abu-Gosh SE, Kolvazon N, Tirosh B, Ringel I, Yavin E. Multiple triphenylphosphonium cations shuttle a hydrophilic peptide into mitochondria. Mol Pharm 2009;6(4):1138–44.
[27] Biswas S, Dodwadkar NS, Deshpande PP, Torchilin VP. Liposomes loaded with paclitaxel and modified with novel triphenylphosphonium-PEG-PE conjugate possess low toxicity, target mitochondria and demonstrate enhanced antitumor effects *in vitro* and *in vivo*. J Control Release 2012;159(3):393–402.
[28] Sahay G, Alakhova DY, Kabanov AV. Endocytosis of nanomedicines. J Control Release 2010;145(3):182–95.
[29] Zhao F, Zhao Y, Liu Y, Chang X, Chen C, Zhao Y. Cellular uptake, intracellular trafficking, and cytotoxicity of nanomaterials. Small 2011;7(10):1322–37.
[30] Sean Marrache SD. Engineering of blended nanoparticle platform for delivery of mitochondria-acting therapeutics. PNAS 2012;109(40):16288–93.
[31] Kim SH, In I, Park SY. PH-responsive NIR-absorbing fluorescent polydopamine with hyaluronic acid for dual targeting and synergistic effects of photothermal and chemotherapy. Biomacromolecules 2017;18(6):1825–35.
[32] Wang ZJ, Kuang X, Shi J, Guo WL, Liu HZ. Targeted delivery of geranylgeranylacetone to mitochondria by triphenylphosphonium modified nanoparticles: a promising strategy to prevent aminoglycoside-induced hearing loss. Biomater Sci 2017;5(9):1800–9.
[33] Funhoff AM, Nostrum CF, Koning GA, Schuurmans-Nieuwenbroek NME, Crommelin DJA, Hennink WE. Endosomal escape of polymeric gene delivery complexes is not always enhanced by polymers buffering at low pH. Biomacromolecules 2004;5:32–9.
[34] Sonawane ND, Szoka FC, Verkman J, Verkman AS. Chloride accumulation and swelling in endosomes enhances DNA transfer by polyamine-DNA polyplexes. J Biol Chem 2003;278(45):44826–31.
[35] Maushagen R, Reers S, Pfannerstill AC, et al. Effects of paclitaxel on permanent head and neck squamous cell carcinoma cell lines and identification of anti-apoptotic caspase 9b. J Cancer Res Clin Oncol 2016;142(6):1261–71.
[36] Lv KT, Gao LJ, Hua X, Li F, Gu Y, Wang W. The role of the globular heads of the C1q receptor in paclitaxel-induced human ovarian cancer cells apoptosis by a mitochondria-dependent pathway. Anticancer Drugs 2017;29(2):1–11.
[37] Park D, Dilda PJ. Mitochondria as targets in angiogenesis inhibition. Mol Aspects Med 2010;31(1):113–31.
[38] Dong K, Yan Y, Wang P, et al. Biodegradable mixed MPEG-SS-2SA/TPGS micelles for triggered intracellular release of paclitaxel and reversing multidrug resistance. Int J Nanomed 2016;11:5109–23.
[39] Rideout D, Bustamante A, Patel J. Mechanism of inhibition of FaDu hypopharyngeal carcinoma cell growth by tetraphenylphosphonium chloride. Int J Cancer: 1994;57:247–53.
[40] Trnka J, Elkalaf M, Andel M. Lipophilic triphenylphosphonium cations inhibit mitochondrial electron transport chain and induce mitochondrial proton leak. PLoS One 2015;10(4):e0121837.
[41] Bielski ER, Zhong Q, Brown M, da Rocha SRP. Effect of the conjugation density of triphenylphosphonium cation on the mitochondrial targeting of poly(amidoamine) dendrimers. Mol Pharm 2015;12(8):3043–53.